Univerzita Karlova v Praze

Matematicko-fyzikální fakulta

BAKALÁŘSKÁ PRÁCE

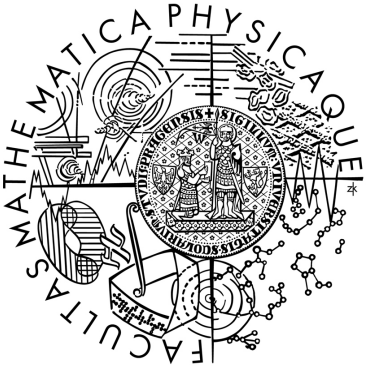

Peter Darebník

Studium transportních jevů v polovodičích na bázi GaAs/AlGaAs pro měření spinového Hallova jevu

Katedra chemické fyziky a optiky

Vedoucí bakalářské práce: doc. RNDr. Petr Němec, Ph.D.

Studijní program: Fyzika, Obecná fyzika

Praha 2014

Rád by som sa poďakoval RNDr. Lukášovi Nádvorníkovi a Mgr. Kamilovi Olejníkovi, Ph.D., za všeobecnú pomoc s touto prácou a za príjemný a ochotný prístup a doc. RNDr. Petrovi Němcovi Ph.D., za vedenie tejto práce. Ing. Vítovi Novákovi, CSc., a Tomášovi Jungwirthovi, Ph.D., a zvyšnému kolektívu oddelenia spintroniky FZÚ AV ČR, v.v.i. za vrelé prijatie do priestorov fyzikálneho ústavu.

Prohlašuji, že jsem tuto bakalářskou práci vypracoval samostatně a výhradně s použitím citovaných pramenů, literatury a dalších odborných zdrojů.

Beru na vědomí, že se na moji práci vztahují práva a povinnosti vyplývající ze zákona č. 121/2000 Sb., autorského zákona v platném znění, zejména skutečnost, že Univerzita Karlova v Praze má právo na uzavření licenční smlouvy o užití této práce jako školního díla podle § 60 odst. 1 autorského zákona.

V Praze dne Peter Darebník

Table of Contents

Název práce: Studium transportních jevů v polovodičích na bázi GaAs/AlGaAs pro měření spinového Hallova jevu

Autor: Peter Darebník
Katedra / Ústav: Katedra chemické fyziky a optiky
Vedoucí bakalářské práce: doc. RNDr. Petr Němec, Ph.D.

Abstrakt: Obsahem této práce je studium transportních jevů v polovodičových strukturách na bázi GaAs/AlGaAs. Tyto heterostruktury se dnes již běžně využívají ke studiu spinového Hallova jevu v pevných látkách, který je možno z části považovat za transportní jev, a proto je důležité znát transportní charakteristiky těchto struktur. Zejména se zaměříme na určení elektronové/děrové pohyblivosti, jelikož tento parametr charakterizuje míru rozptylu ve studovaném materiálu. Cílem je určit, jak se bude mobilita měnit za různých teplot v systému, jehož rozměry jsou srovnatelné se střední volnou dráhou elektronů. Část práce je také věnována teoretickému popisu studovaných jevů a popisu technologie výroby výše uvedených heterostruktur.

Klíčová slova: elektron, spin, Drudeho model, 2DEG, GaAs/AlGaAs heterostruktury

Title: Investigation of transport phenomena in GaAs/AlGaAs based materials for measurements of the spin Hall effect

Author: Peter Darebník
Department: Department of Chemical Physics and Optics
Supervisor: doc. RNDr. Petr Němec, Ph.D.

Abstract: The content of this thesis is the study of transport phenomena in semiconducting structures based on GaAs/AlGaAs. These heterostructures are nowadays widely used for the study of the spin Hall effect, which can be partly considered a transport phenomenon, and it is therefore important to know the transport characteristics of these structures. We will mainly be focusing on electron/hole mobility since this parameter characterizes the scattering rate in the studied material. Our goal is to determine how the mobility will change at different temperatures in a system, which dimensions are comparable to the mean free path of electrons. Part of this thesis is dedicated to theoretical description of the studied phenomena and to the description of manufacturing technology of aforementioned heterostructures.

Keywords: electron, spin, Drude model, 2DEG, GaAs/AlGaAs heterostructures

Introduction

Spin of an electron is an intrinsic property of this elementary particle. Since it does not have any classical analogue it is often overlooked in basic scientific measurements, however it's existence is fundamental for a new, developing field of physics – spintronics. As the name suggests, spintronics is a field, that studies basically all physical phenomena, for which explanation you need a word spin. Ranging from the spin Hall effect, through AMR and GMR to semiconductor antiferromagnets it encompasses fields of optics, optoelectronics and physics of condensed matter.

Roughly two years ago I had the opportunity to work on a student project. The project had to do with measuring the transport properties of gallium arsenide and aluminium gallium arsenide based heterostructures. This thesis is a continuation of that project. My motivation to work on, at the time, such a huge project was obvious. As a second year student of bachelor studies, I had the chance to find out how actual science works.

This thesis is result of almost two years of on and off work at the Institute of Physics AS CR, v.v.i. It is divided in the three main parts. Theoretical one, in which it will be explained how and why semiconductors have a transport properties and a technological and experimental one, in which some light will be shed on how these materials and devices are made and what were the experimental set-up and results.

The goal is to measure the mobility of several GaAs/AlGaAs heterostructures which were patterned by electron lithography with so called Hall-bars – parallel walls which bind the two dimensional electron gas to a rectangular shape with some specified width w. We expect the mobility to start to decrease when width of Hall-bars is approximately the same as mean

free path of electrons in 2DEG and it should continue to drop as we reduce the width even more.

Understanding of the aforementioned goal of this work is critical for proper spin Hall effect measurements, an effect which is vital for detection of spin oriented electric current which is basis for spin-based electronics, that I believe could be the next step in information technology.

Because of long names of some physical phenomena and technological slang, I will use several abbreviations, which I will remind the reader from time to time in the text. These are as follows, SHE – spin Hall effect, 2DEG – two dimensional electron gas, MBE - molecular beam epitaxy, GaAs – gallium arsenide, AlGaAs – aluminium gallium arsenide.

Chapter 1 – Theoretical background

1.1 The Drude model of metals

1.1.1 Basic assumptions of Drude model

In the year 1897 J.J Thompson discovered an elementary particle – electron. This discovery led to a quick explanation of how and why the metals conduct an electrical current. At the turn of a 20th century Paul Drude created a theoretical model which tried to explain the electric conductivity of metals. This more than a century old theory has a wide variety of applications even today. This chapter which explains the transport properties of aluminium/gallium arsenide and gallium arsenide heterostructures will be based on this model as well.

The idea is that the electrons, that are responsible for electric conductivity, are the valence electrons of atoms that create the structure of metal or doped semiconductor. These electrons are not bound so tightly to the core and can therefore break away from it's pull. Every atom supplies several of these electrons. All of them are essentially shared and the so called electron gas is created. This is schematically shown in figure 1, where Z is the number of electrons supplied by each atom, Z_a is the proton number and e is elementary charge. Electron gas density n can be calculated as [1]

$$n = \frac{N}{V} = 6{,}022 \times 10^{23} \frac{Z \rho_m}{A} \quad , \qquad (1)$$

where N is number of electrons in entire volume V of the metal, ρ_m is the mass density of metal and A is the atomic mass number.

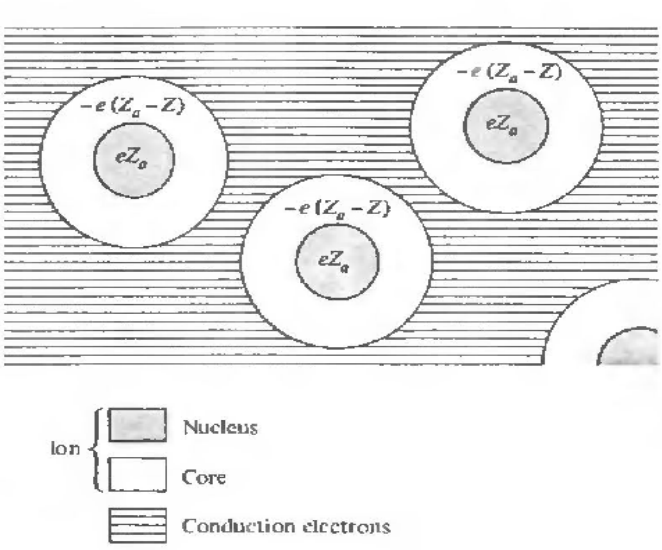

Figure 1: Scheme showing electron gas formation in metal as a product of valence electrons that were able to break away from the atom's core pull. Source [1]

This electron gas is, within this approach, considered to be a classical gas, which is made out of identical solid spheres. This gas acts according to some, so called, basic assumptions. These are as follows [1]:

1. Between collisions, the interaction of a given electron, both with the other electrons and with the ion atomic cores, is neglected. Thus, according to the Newton laws of motion, in the absence of externally applied forces, the electron moves uniformly in the straight line. The neglect of electron-electron interaction is called the independent electron approximation. The neglect of electron-ion interaction is called free electron approximation.
2. Collisions of electrons are instantaneous events that abruptly alter the electron's path and velocity. Drude attributed them to the electrons bouncing off the impenetrable ion cores, which turns out to be true. Electron-electron interaction is usually one of the least significant

scattering mechanisms.

3. Electron undergoes a collision with the probability $1/\tau$. Time τ, is known as a relaxation time, also known as the mean free time. It is the time between collisions of an electron, which means that the electron, on average, is traveling for the time τ, before experiencing a collision. This time is taken to be independent of electron's position and velocity.
4. Electrons are assumed to achieve thermal equilibrium with their surroundings only through collisions.

In the contrary to the title, Drude model, can be used to describe how and why do semiconductors conduct electrical current too. This is because, that semiconductors in general act like metals in a sense, that mechanism of current transport is the same.

1.1.3 The Drude model of metals – Drift and DC conductivity

In the presence of an electrical field $\boldsymbol{E}$ there is a mean velocity of electrons in the crystal, directed opposite to the field. At any point in time, these electrons move in variety of directions, when the field is applied, some particular way is preferred and the net velocity points in the opposite of the field. When no field is applied, no direction of movement is preferred and therefore the net velocity is equal to zero and no electrical current occurs. The process of moving electrons when the electric field is applied is called drift.

The drift velocity v_d is the mean velocity of electrons, that is described above. If we consider the impulse-momentum theorem, that states that impulse $J = force*time$ is equal to the change of momentum we obtain the relation for drift velocity:

$$-e\boldsymbol{E}\tau = m_e^{eff}\boldsymbol{v}_d \;\rightarrow\; \boldsymbol{v}_d = -\frac{e\tau}{m_e^{eff}}\boldsymbol{E} = -\mu\boldsymbol{E} \quad . \tag{2}$$

The quantity $\mu = -e\tau/m_e^{eff}$ is called the electron mobility and it determines how quickly can an electron move through metal or semiconductor when pulled by an electric field. Our goal is to measure this quantity, however, drift velocity can not be measured directly, so we need some other tool, with witch we can determine it.

We begin with current density j [1], which is a measurable entity, defined as an electrical current per unit area of cross section of conductor

$$\boldsymbol{j} = -ne\boldsymbol{v}_d \quad , \tag{3}$$

where n is the number of electrons flowing through the cross section with the mean velocity (the drift velocity) $\boldsymbol{v}_d$.

However there is yet another way how to define the current density $\boldsymbol{j}$. The Drude model states, that electric field $\boldsymbol{E}$ is proportional to current density $\boldsymbol{j}$ with so far undefined constant of proportionality - $\boldsymbol{E} = \rho\boldsymbol{j}$ [1] which means that current density can be defined as:

$$\boldsymbol{j} = \frac{1}{\rho}\boldsymbol{E} = \sigma\boldsymbol{E} \quad , \tag{4}$$

where σ is inverse constant of proportionality. If we substitute for drift velocity $\boldsymbol{v}_d$ in equation 3, and compare this new equation with equation 4, we obtain a relation for this inverse constant:

$$\boldsymbol{j} = -ne\boldsymbol{v}_d = \frac{ne^2\tau}{m_e^{eff}}\boldsymbol{E} \;,\; \boldsymbol{j} = \sigma\boldsymbol{E} \;\rightarrow\; \sigma = \frac{ne^2\tau}{m_e^{eff}} \quad . \tag{5}$$

It is obvious, that there indeed is mobility hidden in the formula 5, that is why we will define the mobility as being proportional to conductivity

$$\mu = -\frac{e}{m_e^{eff}}\tau = -\frac{1}{ne}\sigma \quad . \tag{6}$$

If we define mobility this way, it can be experimentally measured. Since σ is to ratio of electrical current to electrical voltage in unit volume, we called it the conductivity. It can be easily determined and if we also know the value of elementary charge e and the concentration of electrons n, we can determine the mobility. Concentration n is determined from the value of Hall coefficient $R_h = 1/ne$. Understanding of this coefficient will be the main focus of chapter 1.1.3.

1.1.3 Hall effect and magnetoresistance

Consider a metal block which is a subject to externally applied uniform electric field $\boldsymbol{E}$, pointing in direction of +x axis, and a uniform magnetic field $\boldsymbol{B}$, pointing in direction of +z axis as shown in figure 2.

The electric field generates current density j_x pointing in the direction +x. Because of the presence of magnetic field $\boldsymbol{B}$, each electron constituting the current is subject to a Lorentz force $\boldsymbol{F}$ of

$$\boldsymbol{F} = -e\boldsymbol{v}\times\boldsymbol{B} \tag{7}$$

acting in the direction of -y. Since the two sides of metal parallel to the x axis are not electrically connected, electrons can't escape and are therefore accumulating at the -y side of metal. Because of electrical neutrality there is a

positive charge accumulating at the +y side. This leads to an electric field E_y pointing in the direction of -y axis. In the equilibrium state, this field stops further accumulation of charge. This happens when the force resulting from field E_y is equal to Lorentz force

$$E_y = \boldsymbol{v}\,\boldsymbol{B} \quad . \tag{8}$$

This electric field E_y is also called Hall electric field and it can be shown [2] that by solving equations of motions of this system, one can obtain following relation

$$R_H = \frac{E_y}{j_x \boldsymbol{B}} = \frac{\boldsymbol{v}\,\boldsymbol{B}}{-ne\,\boldsymbol{v}\,\boldsymbol{B}} = -\frac{1}{ne} \quad , \tag{9}$$

where we used equation 3 and 8. This gives us crucial tool with witch one can calculate the electron density at a constant current if one knows the value of elementary charge, Hall voltage and a magnetic field that is applied to the sample.

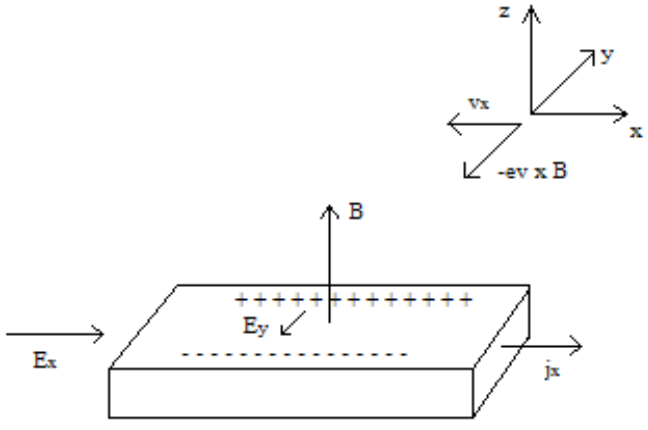

Figure 2: Hall effect scheme showing formation of Hall electric field E_y as a result of magnetic and electric field E_x, that are applied to the sample.

One other quantity is usually defined as well. It is so called magneto-resistance and it is defined as a property of a material to change the value of its longitudinal electrical resistance when external magnetic field is applied [2] or via following relation

$$\rho(B) = \frac{E_x(\boldsymbol{B})}{j_x} \quad . \tag{10}$$

1.1.4 Scattering mechanisms

In thermal equilibrium, conduction band electrons will be in random thermal motion. As these electrons move in the crystal with some thermal velocity v_{th} they scatter (they also can have some drift velocity v_d but the scattering mechanisms would be the same). There are several types of scattering: [4]

1. Atoms in crystal lattice vibrate, because of the thermal energy. Because of quantum mechanical considerations, discrete allowed vibrational states exist which can be modelled as particles called phonons. In a perfect lattice at 0K there is no scattering of this type.
2. Since the semiconductors contain dopants and these dopands tend to get ionized, electrons tend to scatter coulombically on them as well.
3. There are also neutral impurities however scattering caused by them is usually negligible.
4. Electron-electron and electron-hole scattering is significant at high carrier concentrations, however our goal is to occupy only the lowest energy state in potential well, to keep the simplicity of the system (see 1.3.2.1)
5. Crystal defects scattering is also negligible since the crystals we are

using are manufactured with MBE method, which is capable of creating almost perfect crystals.

Out of this five mentioned scattering effects only two first two are significant for our system. As mentioned the first one is minimized when the crystal is at low temperatures and since our experiment was conducted at 4,18K (temperature of liquid He) this effect is negligible. However the second scattering effect is present even at low temperatures. It can be minimized using 2DEG, because of reasons explained in chapter 1.3.2.1.

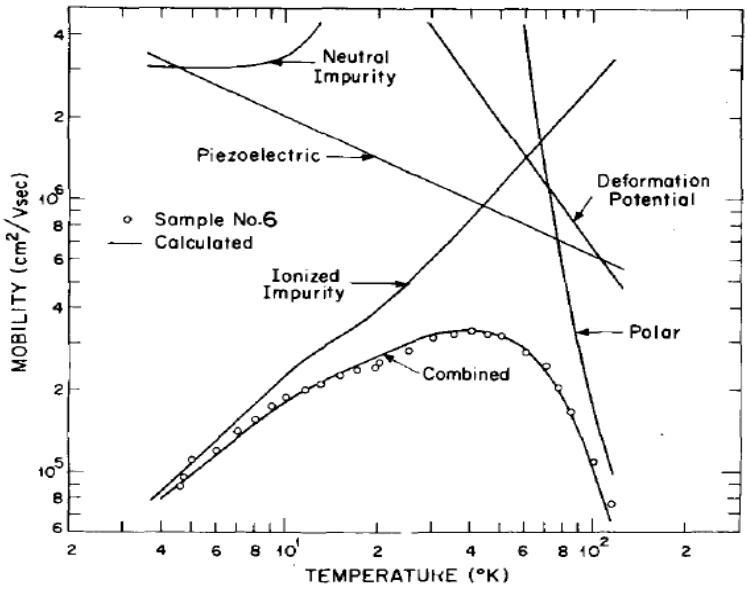

Figure 3: This graph depicts temperature dependence of mobility in bulk doped semiconductor. At room temperature the mobility is low, but it raises as temperature lowers, because the crystal lattice stops vibrating. However at even lower temperatures the scattering on impurities occurs. Source [3]

It is now obvious that if we use a 2DEG in a crystal cooled to low temperatures we can obtain high mobilities because the electrons do not scatter so much.

In the figures 3 and 4 one can see how mobility behaves in bulk semiconductor and in 2DEG when temperature is changed.

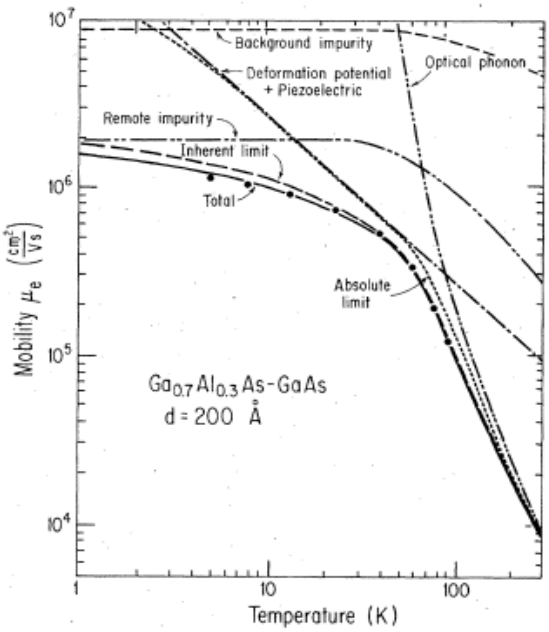

Figure 4: This graph is similar to figure 3, however it shows temperature dependence of mobility specifically for 2DEG, where scattering on phonons is suppressed. Source [4]

1.2 Boltzmann and Fermi-Dirac distributions

There are three very well know statistical distributions of particles in a system. The classical one, the Boltzmann distribution, is typically used to describe a system which temperature is in order of hundreds of Kelvins. Other two – the Fermi-Dirac and Bose-Einstein distributions are used for description of quantum systems that are composed either from fermions or bosons, typically at a temperature in order of Kelvins. In this section, we will take a closer look at the first two – Boltzmann and Fermi-Dirac distributions.

Boltzmann distribution is defined as [5]

$$f_B(E) = A * e^{-\frac{E}{kT}} \quad , \tag{11}$$

where E is energy, k is the Boltzmann constant, T is absolute temperature and

A is a normalization factor – the partition function $1/Z$. Fermi-Dirac distribution can be written as [6]

$$f_{FD} = \frac{1}{1+e^{\frac{E-E_F}{kT}}} \quad , \tag{12}$$

where all parameters are the same as in equation 11 and E_F is the Fermi energy defined as the point where the value of Fermi-Dirac function is one half

$$f_{FD}(E_F) = \frac{1}{2} \quad . \tag{13}$$

1.2.1 From Boltzman to velocity Maxwell-Boltzman distribution

Let us consider the Boltzmann distribution 11 as a function of one dimensional velocity v_z, where $E = ½\, mv_z^2$

$$f_B(v_z) = A * e^{\frac{-mv_z^2}{2kT}} \quad , \tag{14}$$

where m is a mass of a particle. Since this distribution needs to be normalized so the probability of finding a particle with some velocity is one, we need to integrate equation 14 from minus infinity to plus infinity. In order to do this we will make use of the following equation

$$\int_{-\infty}^{+\infty} e^{-x^2} dx = \sqrt{\pi} \quad . \tag{15}$$

If we now integrate Boltzmann distribution from minus infinity to plus infinity and we substitute for $x = (m/2kT)^{-1/2} v_z$ we obtain

$$A\int_{-\infty}^{+\infty} e^{\frac{-mv_z^2}{2kT}} dv_z = A\sqrt{\frac{2kT}{m}}\int_{-\infty}^{+\infty} e^{-x^2} dx = A\sqrt{\frac{2kT}{m}}\sqrt{\pi} = 1 \rightarrow A = \sqrt{\frac{m}{2\pi kT}} \quad . \qquad (16)$$

Note that we only received 1D velocity distribution. In order to have three dimensional one, we need to write velocity as $v^2 = v_x^2 + v_y^2 + v_z^2$. This way the normalizing constant A will be to the power of three. Moreover we need to multiply the distribution by a factor of $4\pi v^2$ to account for the density of velocity states available to particles. Finally we obtain three dimensional velocity distribution written as

$$f_{MB}(v) = 4\pi v^2 \left(\frac{m}{2\pi kT}\right)^{3/2} . e^{\frac{-mv^2}{2kT}} \quad . \qquad (17)$$

Equation 17 is graphically shown in figure 5 for set of three different temperatures. Note that both x and y axes are in relative scales. However this does not matter since we only wanted to compare the number of particles which travel at the most probable velocity to the rest. There are two types of velocities that are of interest here. First is the most probable velocity v_{max} and the second is the average velocity of particle $\langle v \rangle = \int v.f_{MB}(v)dv$. It can be seen, that at low temperatures they are roughly equal, but at high temperatures they are different. This observation will be important later, in the chapter 3 where experimental results will be discussed.

We can calculate the most probable velocity v_{max} as $df_{MB}(v)/dv = 0$, however what is really of our interest is the average velocity $\langle v \rangle$ which can be calculated as

$$\langle v \rangle = \int_0^\infty v\, f_{MB}(v)\, dv = \sqrt{\frac{8\,RT}{\pi\, M}} \quad . \tag{18}$$

Mean square velocity is then

$$\langle v^2 \rangle = \int_0^\infty v^2\, f_{MB}(v)\, dv = \frac{3\,RT}{M} \quad . \tag{19}$$

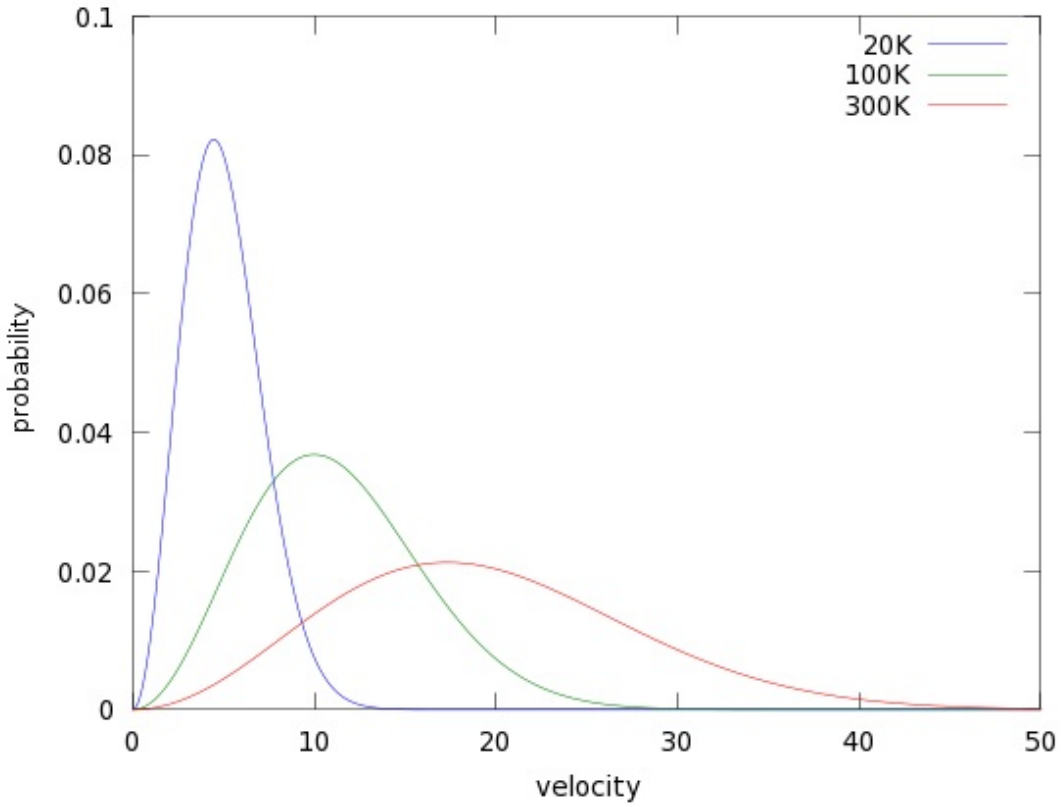

Figure 5: Maxwell-Boltzmann velocity distribution in relative scales. One can see that at low temperatures narrower spectrum of velocities is available as opposed to high temperatures.

1.2.2 From Fermi-Dirac to Boltzmann distribution

Let us consider equations 11 and 12. At a first glance some similarities can be seen. At high temperatures $E - E_F > kT \Rightarrow exp((E - E_F)/kT) \gg 1$ and we

immediately see that factor 1 is negligible since exponential function takes precedent. We can say that at high temperatures Fermi-Dirac distribution transforms to the Boltzmann distribution.

This fact can be graphically shown but first we need to realize several things. First is, that Fermi energy E_F is temperature dependent if the concentration of carriers in a system is constant (which is the case in our system is as will be shown later on in chapter 3). To keep the concentration constant, function 12 needs to be normalized and only free parameter in equation 20 is E_F

$$const. = \int_0^{+\infty} \frac{1}{e^{(\frac{E-E_F}{kT})}+1} \quad , \tag{20}$$

where *const.* is a constant that takes into the account that DOS(E) = const. and it is a result of an integral form zero to plus infinity of equation 12 at temperature T = 0K. It is also the number to which we need to normalize Fermi-Dirac distribution at a temperatures different from 0K. And as have been said, the only way to do that is to change the only free parameter E_F which is therefore temperature dependent.

Last thing we need to think about is what we consider high temperatures. E_F is lowering as the temperature is increasing which means that at some point it will go from being positive number to being a negative number. Temperature at which this occurs is close to the Fermi temperature defined as $E_F = kT_F$ and temperatures above this are for all our needs and purposes called high temperatures.

Now we have all we need to graphically show how Fermi-Dirac distribution transfers to the Boltzmann distribution. Let's take a look at $E_F(T)$

dependence in a figure 6 first. As predicted, E_F indeed decreases with rising temperature and at some point it crosses zero zero line, which is indicated.

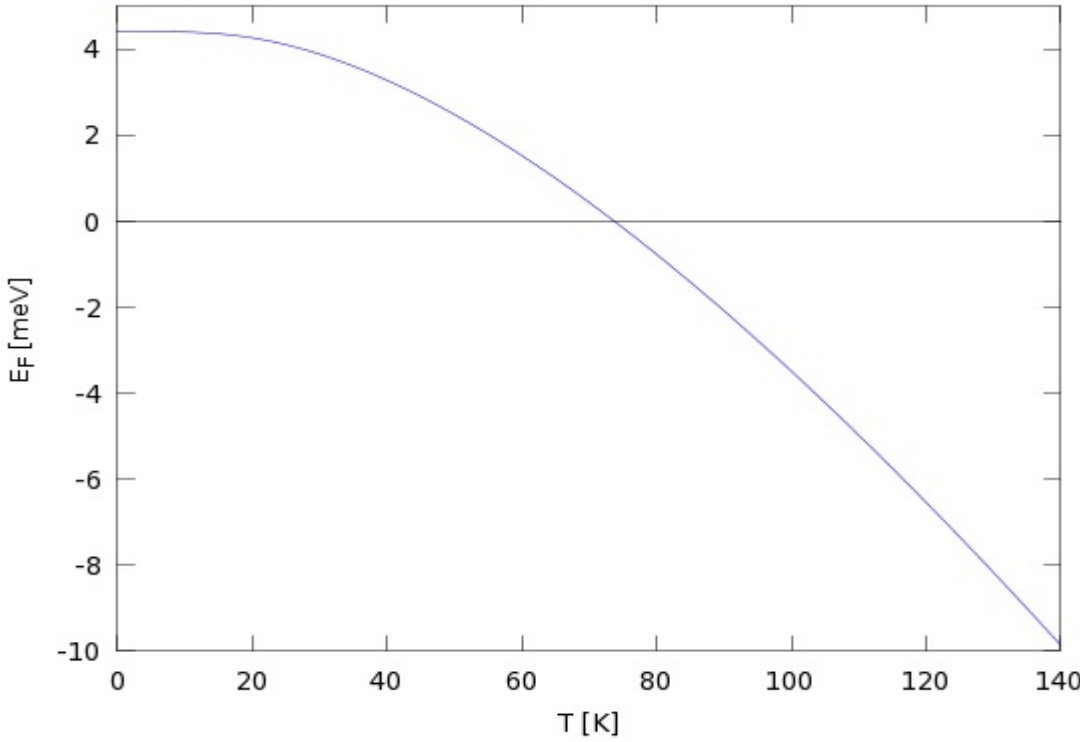

Figure 6: Temperature dependence of E_F. It is shown that Fermi energy lowers with temperature. Because of the definition of Fermi temperature above, we can define low and high temperatures. This graph is a result of numerical solution of equation 20.

That means that at this point the system has already reached the Fermi temperature. For this particular sample it is about 75K, and the Fermi temperature is about 50K. Following graph, in figure 7 shows, how Fermi-Dirac distribution evolves with rising temperature. Because of the change of E_F curves are shifted to the left with respect to x axis. This means that the inflex point (point where $E = E_F$) is also moving to the left and when it intersects y axis we can say, that the system can be approximated by Maxwell distribution instead of the Fermi-Dirac distribution. Comparison of exponentially decreasing part of Fermi-Dirac distribution and entire Boltzmann distribution for $A = 1$ and at a temperature of 100K (temperature

above the Fermi temperature) is shown in figure 8.

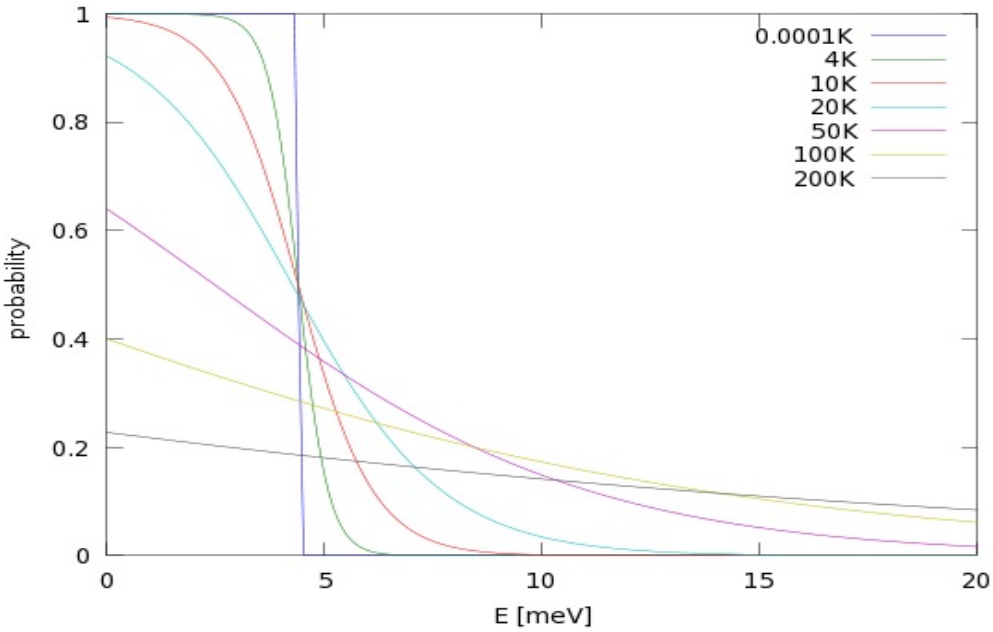

Figure 7: Temperature development of Fermi-Dirac distribution. Note that with rising temperature curves move to the left. This is because of temperature dependent Fermi energy and it leads to the fact, that at high enough temperature only exponentially decreasing part of distribution remains – we obtain the Boltzmann distribution.

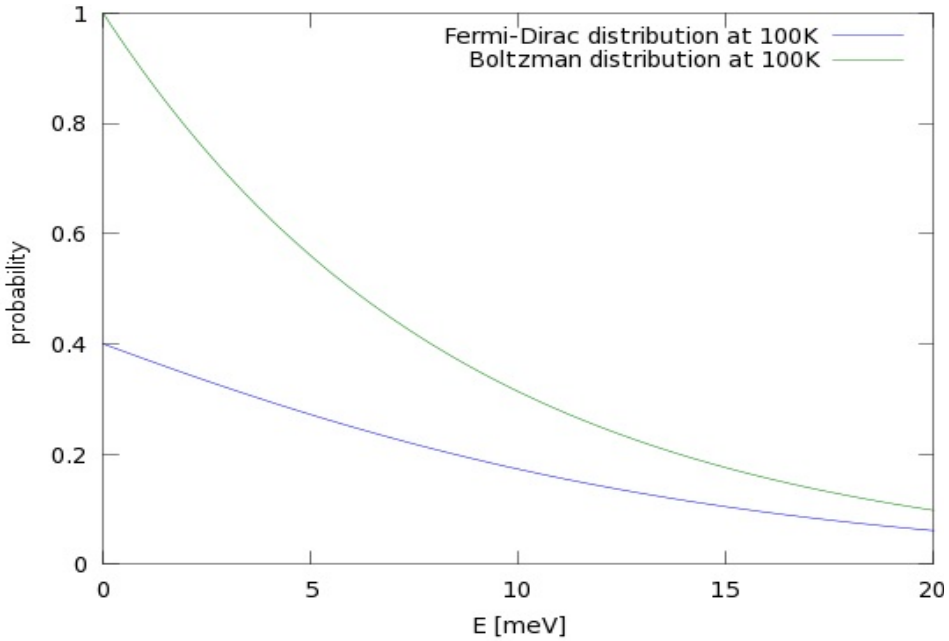

Figure 8: Comparison of Fermi-Dirac and Boltzmann distribution at 100K showing, that at this temperature they are equivalent because both are exponentially decreasing distributions.

1.3. Other transport effects

1.3.1 Transport in systems described by Boltzmann distribution

Diffusion is a process during which there is a particle flux from the region of high concentration of particles (in our case, electrons or holes) to surrounding regions, where the concentration of particles is lower (this can be seen in figure 9, which shows carrier concentration in one dimensional

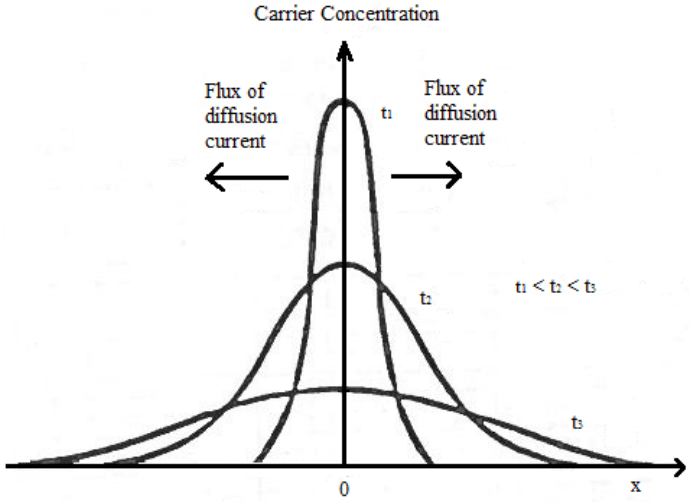

Figure 9: Carrier concentration in 1D space over time. This scheme shows that particles flow from regions of high concentration to regions with low concentration of particles.

space over time). It is governed by the Fick's first low which states, that the magnitude of flux of carriers of charge, ϕ, is proportional to the concentration gradient [1]:

$$\phi = -D\frac{\partial c}{\partial x} \quad , \tag{21}$$

where D is diffusion coefficient and c is a concentration of charge carriers.

Equation 21, of course governs one dimensional case.

The diffusion current can therefore be written as

$$I = eAD_n \frac{\partial n}{\partial x} - eAD_p \frac{\partial p}{\partial x} \quad , \tag{22}$$

where D_n and D_p are diffusion coefficients of electrons and holes, e is elementary charge, A is one dimensional area and n and p are electron and hole concentrations.

If we want to determine the diffusion coefficient, we first need to calculate the thermal velocity of particles. We will do so thanks to the Maxwell-Boltzmann velocity distribution 17 in ideal gas. In section 1.2.1 we already calculated this velocity in equation 19. If we divide this equation by two and multiply by M, we obtain widely known equation from statistical mechanics for the average energy of a particle of ideal gas in three dimensions:

$$\frac{1}{2} m_e^{eff} v_{th}^2 = \frac{3}{2} RT \quad , \tag{23}$$

where M, in case of electron gas, which is considered to be ideal gas (see 1.1.1) can be substituted for m_e^{eff}, which is effective electron mass.

Let us go back to the diffusion coefficient now. Consider an electron diffusion with carrier concentration $n(x)$ as shown in figure 10. Rate of electrons crossing position $x = 0$ from left is $n(-l)v_{th}/2$ and from right is $n(l)v_{th}/2$, where $l = v_{th}\tau$ is mean free path of an electron (τ is mean free time between collisions, see section 1.1.1). Particle flux at this position therefore is

$$\phi = \frac{1}{2} v_{th}[n(-l) - n(l)] = \frac{1}{2} v_{th}\left[\left(n(0) - \frac{\partial n}{\partial x} l\right) - \left(n(0) + \frac{\partial n}{\partial x} l\right)\right] = -v_{th}\, l \frac{\partial n}{\partial x} \qquad (24)$$

if we compare equation 24, with the Fick's law equation 21, we immediately see, that the diffusion coefficient in case of electrons, can be written as

$$D_n = v_{th}\, l = v_{th} \cdot v_{th} \tau = \tau \frac{kT}{m_e^{eff}} = \frac{kT}{q} \mu \quad . \qquad (25)$$

Obviously we substituted for $l = v_{th}\tau$, then we substituted for v_{th}^2 from equation 23, which in 1D has *1/2* on the right side instead of *3/2* (this is called equipartition theorem).

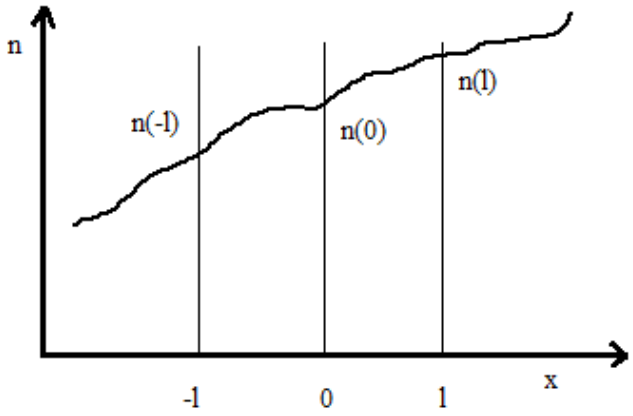

Figure 10: Carrier concentration *n*, as a function of x, showing that there is lower concentration at the point -l, that it is at the point l.

Another thing we can do now, is to define current density *j* in yet another way. It can be defined as electric current per unit area of cross section, and therefore can be written as

$$j = e \times \phi = e D_n \frac{\partial n}{\partial x} \quad , \tag{26}$$

where ϕ is the electron flux from equation 24 which can be rewritten according to it's definition.

Lastly, we can rewrite the mean free path of electrons *l*, as

$$D_n = v_{th} l = \frac{l^2}{\tau} \rightarrow l = \sqrt{D_n \tau} \quad , \tag{27}$$

where we used similar substitutions as in equation 25.

In conclusion, in this chapter, we derived the Einstein relation 25 and we also redefined the current density *j* 26.

1.3.2 Transport in systems described by Fermi-Dirac distribution

1.3.2.1 2DEG and its formation in GaAs/AlGaAs

One of the thinnest conducting layers of material is two-dimensional electron gas, 2DEG. It is created at the interface of two semi-insulating semiconductors.

The general idea is that the top and bottom materials have different band structures, one's energy gap is larger than the others. Because of the gap difference, there is a potential step at their interface. In our case these are GaAs and AlGaAs. These are typical crystals grown epitaxially – layer by layer, using MBE method (see section 2.1). At the room temperature entire volume of this structure can conduct electricity, because of thermal excitation of electrons above the energy gap between the dopant level and conduction level, therefore the interface is ignored. However what is really going on is

that GaAs is undoped and AlGaAs is n-doped semiconductor, and thus the electrostatics creates a triangular potential well at the interface. The potential at this interface is shown in the figure 11. At low temperatures electrons do not have sufficient energy to pass the energy gap formed by the interface and they are therefore locked in this potential well.

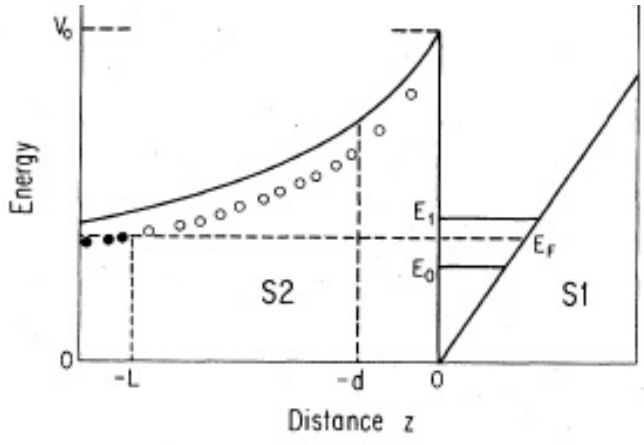

Figure 11: Shape of the potential at AlGaAs/GaAs interface. S1 and S2 are schematically shown semiconductors. Because of this shape, at the point 0, there is triangular potential well created. Source [4]

The electrons are free to move in the two dimensions along the interface, however in the direction perpendicular to it they are bounded in the energy states E_n that are given by the shape of the potential well. Intrinsic energy of electrons is therefore given by formula [7]

$$E_n(\vec{k}) = \frac{\hbar^2 k^2}{2\mathrm{m}_e^{eff}} + E_n \quad , \tag{28}$$

where $\boldsymbol{k}$ is the wave vector of electron and m_e^{eff} is the effective mass of electron.

If the concentration of charge carriers is sufficiently small, they only occupy the lowest energy states E_0 and the 2DEG is created. If not, the

electronic properties (such as quantum Hall effect) can be much more complex.

It is clear that in systems like these, we can obtain high mobilities. It is because, as mentioned in chapter 1.1.4, there are two main scattering mechanisms. Scattering on phonons is suppressed if temperature is decreased, however the scattering on charged dopants is present even at low temperatures. But since the 2DEG is created at the interface between the atomic layers of GaAs/AlGaAs it is relatively distant (approximately the point -d in figure 11) from these dopants. Therefore the second mechanism is basically non-existent in this scenario and the mobility raises dramatically in 2DEG. It is worth noting that there are two competing factors when speaking about second scattering mechanism. Further the gas is from these ionized dopants the scattering is more suppressed, however further it is the lower the mobility is. There of course is an optimum between these factors, but it is not the point of this note.

1.3.2.2 Diffusion at low temperatures, mean free path l_F and density of states

In order to answer the question, what is the mean free path $l = v_{th}\tau$ of electrons, we only need to determine the velocity v_{th} (since we know that τ is proportional to mobility). It has been stated that this can not be directly measured and while we have derived theoretical prediction given by equation 23, it is not correct at low temperatures.

At low temperatures almost all thermal energy of electrons is lost and the quantum mechanical properties arise. The thermal velocity v_{th} is, at low temperatures, referred to as Fermi velocity v_F. It is quantized and proportional to Fermi energy – energy of the highest occupied energy state of

quantum system described by the Fermi-Dirac distribution at 0K. In order to calculate the Fermi velocity, we must first determine the density of states of two dimensional quantum system.

Definition of density of states (DOS) is that it is a number of states per interval of energy available to be occupied by electrons. Mathematically it can be written as

$$dn = DOS(E)\,dE \quad . \tag{29}$$

We know that the relation between energy E and $\boldsymbol{k}$ vector is as follows

$$E = \frac{\hbar^2 k^2}{2m} \rightarrow E_F = \frac{\hbar^2 k_F^2}{2m} \quad , \tag{30}$$

which means that there is a parabolic relation between the two. This is schematically shown for a one dimensional case in figure 12.

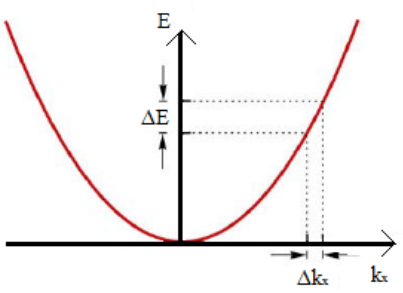

Figure 12: Parabolic relation between energy and k vector. If we increase k vector by Δk, energy does not increase by the same amount.

The idea is that at 0K only the electrons which occupy the highest energy states can conduct electricity. Therefore only highest energy states are

of interest to us. This means that if we were to ,,fill,, this parabola with electrons, only the surface electrons would conduct electricity. This surface would in this case be a line perpendicular to axis E going from left point of intersection with parabola to right point of intersection with parabola. The number of electrons that would fit in this line is corresponding to the DOS(E_F) (every electron has it's ,, DOS($\boldsymbol{k}$) size,, $(V/2\pi)^j$ in $\boldsymbol{k}$ vector space, where j is the dimension of $\boldsymbol{k}$-space and V is the volume). For our needs however, we need to move from one dimensional case to two dimensional case, since our quantum system is 2DEG. This means that $\boldsymbol{k}$ vector would not be one dimensional as it is in figure 12, but it would be two dimensional. The resulting graph would be a rotational paraboloid, and the highest energies would correspond to a disk. This also means that with every increase of energy by ΔE, the k space would not increase by $\Delta\boldsymbol{k}$, but the radius of the disk would increase with means that it's surface would increase by an annulus of size $2\pi\boldsymbol{k}\Delta\boldsymbol{k}$. In conclusion we obtain

$$N = DOS(\boldsymbol{k})\,2\pi\,k\,dk = \frac{V^2}{(2\pi)^2}2\pi\,k\,dk = \frac{V^2}{2\pi}k\,dk = dnV^2 \;\rightarrow\; dn = \frac{k\,dk}{2\pi} \quad , \quad (31)$$

Where V^2 is the volume in 2D. If we substitute the left side of equation 31 with the right side of equation 29 we obtain

$$DOS(E)\,dE = \frac{kdk}{2\pi} \;\rightarrow\; DOS(E)^{-1} = \frac{2\pi}{k}\frac{dE}{dk} = \frac{2\pi}{k\dfrac{m_e^{eff}}{\hbar^2 k}} = \frac{2\pi\hbar^2}{m_e^{eff}} \quad , \quad (32)$$

where the derivative was calculated from equation 30.

The concentration of charge carriers n, at a certain energy level is

according to equation 29

$$n = DOS(E)E = \frac{m_e^{eff}}{2\pi\hbar^2}\frac{\hbar^2 k^2}{2 m_e^{eff}} = \frac{k^2}{4\pi}\times 2 \quad . \tag{33}$$

Final multiplication by two is because of the spin of the electron. If we now realize that we can determine the Fermi velocity from the kinetic energy equation $\frac{1}{2}mv_F^2$ and compare it to equation 30 where we substitute from equation 33 for $\boldsymbol{k_F}$ vector we obtain

$$v_F = \frac{\hbar}{m_e^{eff}}\sqrt{2\pi n} \quad . \tag{34}$$

Now we know all we need, since mean free path $l_F = v_F\tau$ and time $\tau = \mu m_e^{eff}/e$ we obtain the final equation for the mean free path

$$l_F = \frac{\hbar\mu}{e}\sqrt{2\pi n} \quad , \tag{35}$$

which is only valid if T = 0K and only if our system can be described by Fermi-Dirac distribution.

From this result we formulate the idea is that when mean free path l_F of electrons is larger than Hall-bar width, scattering on walls takes precedent and mobility decreases. This idea is a basis to the conducted experiment.

1.4 Conclusion – Theoretical part

It is obvious that the theory behind the phenomena has a great deal of complexity. Therefore it's point is not to explain but rather to describe and to give some foundation to the idea that mobility can change simply because of some spatial limitations. Several key relations which are the basis for this idea were explained or derived in this chapter, including equations 6, 9, 23 or 35.

Chapter 2 – Technological process

2.1 Molecular beam epitaxy

Molecular beam epitaxy or MBE is one of several crystal deposition methods. It's scheme is shown in the figure 13.

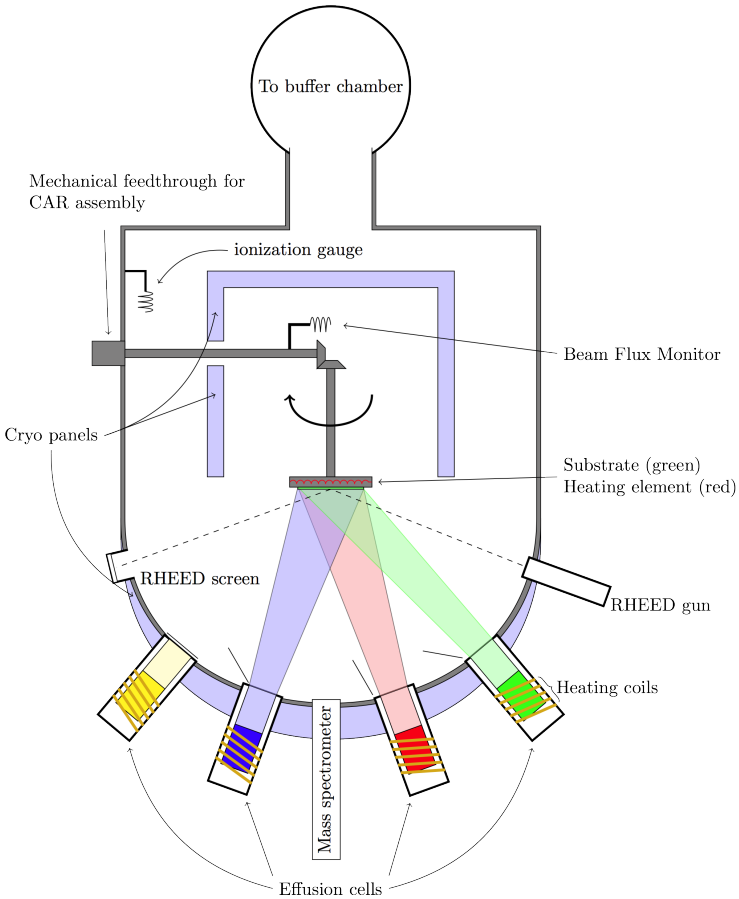

Figure 13: Scheme of MBE showing how effusion cells evaporate required elements at a substrate. It's thickness is controlled by RHEED gun, which is also shown. Source [8]

The most important element of MBE are effusion cells. Within these cells there are needed elements of for example, gallium, arsenic or aluminium in ultra-pure form. These cells are then heated to high

temperatures (thousands of °C) until sublimation starts. The former solid elements begin to evaporate at a certain rate. These gases hit the substrate and the crystal grows.

Substrate is commercially available wafer of GaAs, it is placed inside of a high vacuum chamber. Typical vacuum for this system is about 10^{-8} Pa. The vacuum is maintained by cryo-pumps. These pumps cool the walls of vacuum chamber with liquid nitrogen to 77K and any atom that hits them is gradually slowed down, until they ,,freeze,, and stick to the walls.

The crystal growth is controlled by RHEED method. It is used to precisely measure the thickness of grown crystal which can be determined down to one layer of atoms. Typical deposition rate is less than 3000 nm per hour.

2.2 Photolithography and electron lithography

The goal of this technology it to create patterns on the crystal bulk (substrate created f.e. with MBE method). These patterns are basically trenches in the crystalline structure of the bulk. The process will be explained with the help of simplified scheme in figure 14. In this figure the wafer is divided into the oxide and substrate part. Our bulk is made out of GaAs and AlGaAs, which means that we can imagine the oxide part being AlGaAs and the substrate part being GaAs.

First we need to have properly prepared bulk. What that means is that the wafer is cleaned and a chemical that promotes adhesion is applied to the surface.

Next the chemical called photo-resist is applied. There are basically two types of these resists. Negative or positive ones. The first hardens when

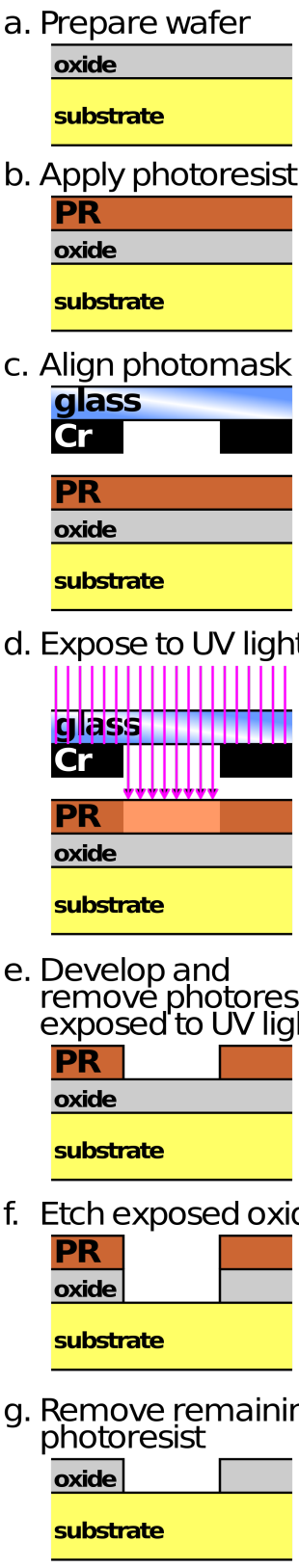

Figure 14: Simplified scheme of litography. Source [9]

exposed to UV light, the second hardens when not exposed to the light.

One way or another we can create desired pattern with the use of photo-mask. This mask hides the parts of resist which we don't want to expose to the light (or which we want to expose in the case of positive resist).

In the next step we expose the sample. By doing so we harden the resist in the specified places.

With the use of deveoper we remove the resist which we did not expose. This leaves us with bulk that is somewhere covered with resist.

Next step is etching. During this process we physically create trenches into the surface of the sample. There are again two ways how to etch – dry or wet. When wet etching the sample is submerged into the solution of phosphoric acid and by chemical reaction we remove a portion of the crystal. If dry etching, the sample is placed into the etching machine, where the role of H_3PO_4 is taken by silicone tetrachloride (and Ar^+), a gas that again chemically removes a portion of the crystal.

Last thing to do is to remove the remaining resist with acetone.

The principle of electron lithography [10] is

the same as it is with photo-lithography, however the role of light is taken by a beam of electrons and we use electron sensitive resist, instead of photo sensitive one.

Both of these technologies have their limitations in how small patterns they can create. Photo-lithography is viable for the dimension down to one micrometer (in extreme cases tens to hundreds of nanometres), but it can illuminate a large area, electron lithography is viable down to tens of nanometres.

2.3 Manufacturing of contacts

For actual measurements there needs to be some way with which one can create a current in the crystal or measure the voltage needed to generate such current. One of these ways is a method similar to effusion cells at MBE. Again we place the bulk into the vacuum chamber, but this time, the role of effusion cell is taken by simple heating element. A piece of AuGe – alloy of gold and germanium, is placed atop of this element. As the temperature rises the AuGe begins to evaporate and condensates on the surface of bulk. Usually we don't want to expose entire surface of the bulk, therefore we need to cover appropriate parts of the bulk by a method described in section 2.2. In fact we use the photo-resist again to cover areas we need. The idea is that the entire surface of the bulk is always exposed, but when we place the device in a solvent that dissolves said resist, we are left only with areas that were not covered by resist before exposure. This process is called lift-off – areas where AuGe stuck to the surface covered by resist are lifted off the surface of the bulk when the resist dissolves.

2.4 Manufacturing of devices

The actual devices were manufactured using the technologies described in previous pages. The devices are 5x5 mm^2 in size and they contain 9 sub-devices in the grid of 3x3, however only 8 of them are usable for experimental purposes, 9^{th} is so called dumb device and it is used as a testing device during manufacture process and for holding the chip. One particular sub-device is shown in figure 15.

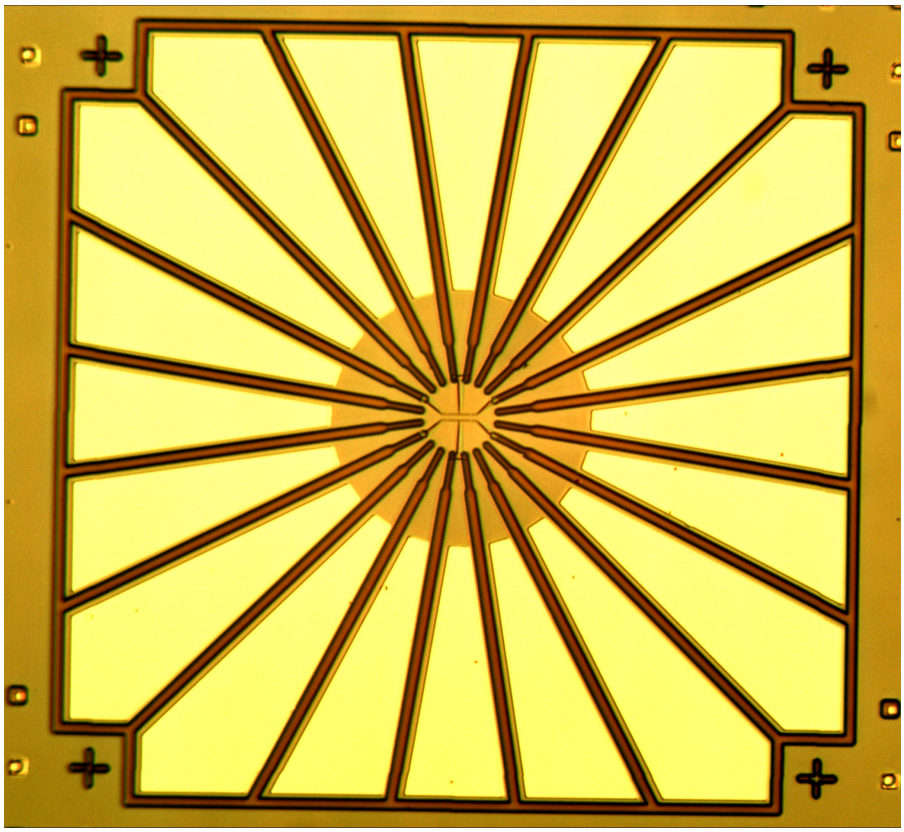

Figure 15: One of manufactured subdevices. The larges elements are the contacts. In the middle there is Hall-bar. The picture was taken by an optical microscope equipped with a camera. Magnified approximately 115x.

It is worth noting that due to a use of optical microscope with a camera, colours are distorted and they do not represent actual colors. The

outside square with the rays pointing to the centre of device are the biggest trenches. They were created using photo-lithography. In the centre, inside the ring, there is actual Hall-bar. Close-up of the Hall-bar is shown in figure 16, where you can see the description of the Hall-bar. It has a width w, there is current I flowing through it and you can see the points at which the Hall voltage V_h and current voltage V, was measured. This Hall-bar was created using the electron lithography. It's width ranges from 1 to 30 μm.

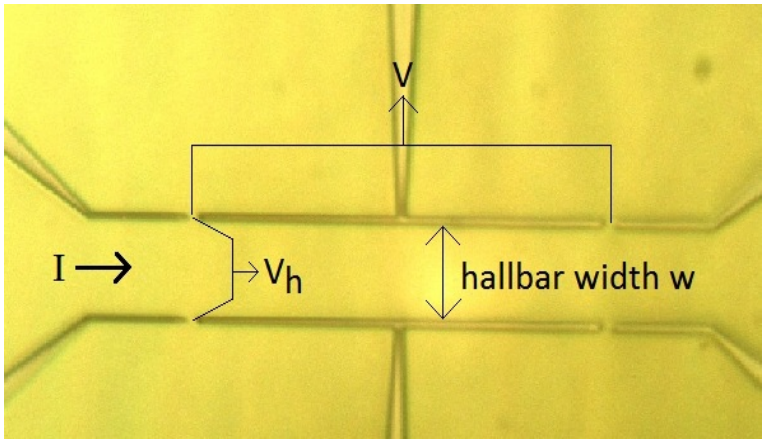

Figure 16: Closeup of the Hall-bar showing the source of the current and contacts with which Hall and longitudinal voltage was measured. The picture was taken by an optical microscope equipped with a camera.

The largest areas, which are white-ish in colour, are AuGe contacts. They were created using method described in section 2.3. These contacts need to be annealed first. This fact is obvious if we take in to the account that the 2DEG is created at the GaAs/AlGaAs interface, which is about 150 nm beneath the surface. That is why if not annealed, they would not work at low temperatures. By annealing we force the AuGe alloy to loose it's integrity to some extent. When hot, Ge atoms diffuse through the crystal structure of AlGaAs. These atoms ,,grab,, the Au atoms and through this diffusion root-like wires are created, connecting the surface of the device with it's inside.

Problem is that we need to anneal the device only for some relatively exact time, and at some relatively precise temperature. If one was to anneal too short, roots would not be deep enough and the contacts would not work. If annealing for too long, roots would be too deep and contacts would not work properly.

2.5 Conclusion – technological part

It can be easily seen, that manufacturing a device is impressive yet difficult. During manufacture, there can be a lot of mishaps and a lot of work can be destroyed. However if careful, functioning devices can be made. Even though, there is about 30 percent chance that the device would not work properly or not at all. That is the reason for why some data points are missing. Reader can observe that in chapter 3.

Chapter 3 – Experiment

3.1 Experimental setup

All together, two different types of materials were used. Codenamed E091 and G096. Both of them are capable of generating 2DEG, therefore they are perfect for desired measurements. Each wafer, when created, is tested an it's mobility determined. Therefore we had a value of mobility that we were expecting from the measurements. In case of E091 it was about 10^6 $cm^2/V.s$ at a concentration of n = 2,3x10^{11} cm^{-2}, in case of G096 it was roughly 5.10^5 $cm^2/V.s$ at a concentration of n = 1,24x10^{11} cm^{-2}. Based on the equation 35, we knew the mean free electron path was about 6-8 μm for wafer E091 and about 3 μm for G096, which are the Hall-bar widths at which we expected the mobility to drop.

Due to some technical difficulties, each material was measured somewhat differently. Material E091 was practically always measured in a set-up a), material G096 was measured in set-up b) as well as in set-up a). The explanation of set-ups is as follows:

a) This is the simpler set-up. It's basis is 65 litre jerry can containing liquid helium at a temperature of about 4,2K. The device was connected through specialized socket to a cue through which a set of cables is going to volt meters. This cue was suspended in the air on a crane which would slowly lower it to the jerry can. Another crucial component is a supra-conducting magnet able to generate fields up to 3,5T [11]. It was placed to helium first, so when to cue went down, the magnet was already inside. This way it is possible to control the temperature of the device and apply the magnetic field to it when it's in the down position completely.

b) This set-up contains cryostat, a device that is, thanks to the in build heater, capable of changing and maintaining the temperature in the interval from 2K to 300K. Cryostat also contains a magnet, with which operator can apply a magnetic field to the device.

3.2 Experimental results

3.2.1 Results obtained at 4K

According to theoretical assumptions in section 1.3.2.2 we expect the mobility to drop when the Hall-bar width w is comparable to mean free path of electrons l_F, defined in equation 35. This can be seen in figure 17, which shows $\mu(w)$ dependence for sample E091.

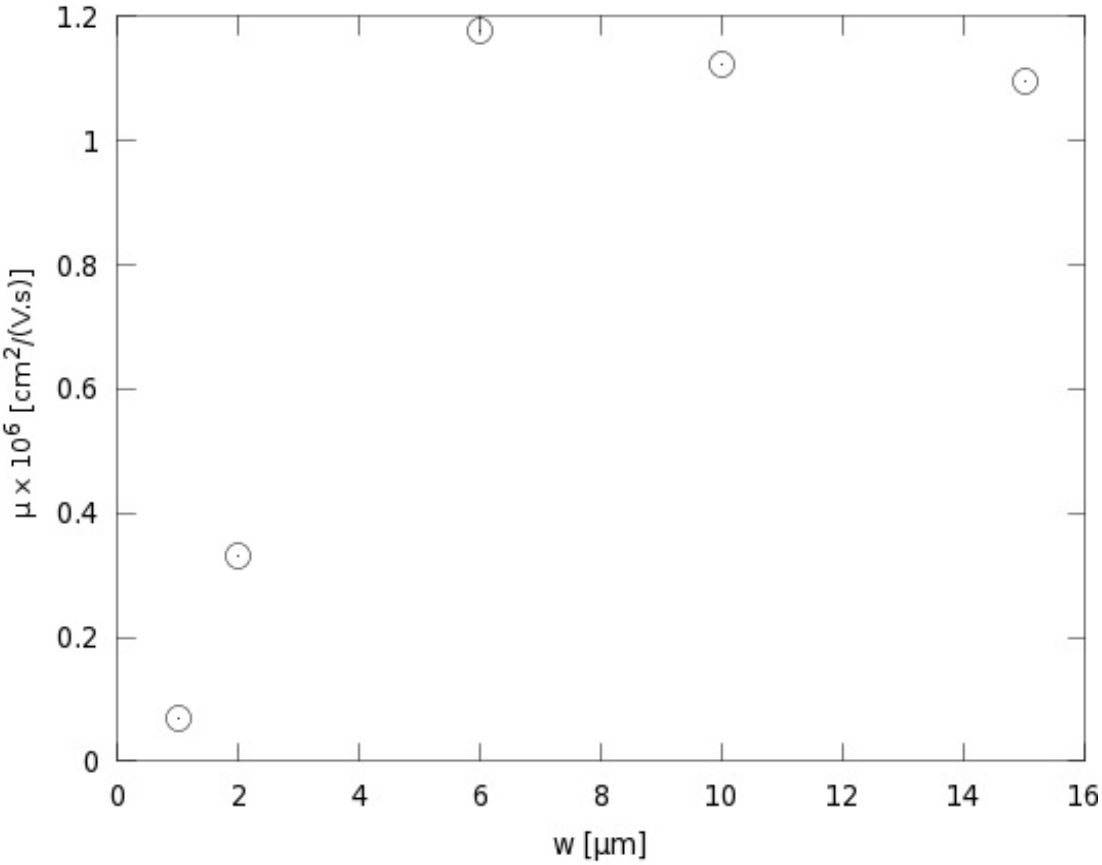

Figure 17: μ(w) dependence for E091 sample at 4K showing that mobility drops at expected value of width – 6 μm.

Figure 17 shows several very important results. First of them being, that the mobility indeed drops beyond 6 micrometer point which is theoretically predicted mean free path of electrons. With this, we have experimentally proven that the idea of reduction of mobility because of spatial limitations is true. We have also shown that by this method we are able to determine the minimum width of Hall-bar, at which the mobility is still unaffected. However in figure 17 it can be seen that it contains only 5 data points while in chapter 2 it has been stated that each batch of devices contains 8 measurable sub-devices. It is because 2 of these 8 sub-devices were not functioning properly or not at all and one sub-device had a Hall-bar width of 30 micrometers and therefore it is not important to include it in this graph.

The fact that 25% of devices were not functioning is unpleasant. Missing widths are 4 and 8 micrometers. Width 4 μm is particularly important since it is the threshold between limited and unlimited mean free path. Still, some conclusions can be made, because devices with widths 1 and 2 μm were working. Mobility indeed drops when Hall-bar width is lowered and this drop can be quite significant. For device with Hall-bar width 1 μm this drop is by a factor of 10.

Figure 17 only shows one particular dependence. It is for a device with mobility of one million $cm^2/V.s$ (if 2DEG is not restricted) and at one particular temperature. If we wanted to investigate this phenomena with respect to varying wafer mobility we would need very large amount of samples (in order of hundreds) and since manufacturing one batch of device take up to 2 days of work it would prove to be time consuming. Therefore a new way of measurements was developed. It will be described in the sections that are to follow.

3.2.2 Temperature dependent measurements

The next experimental approach benefits from dependence of mobility on temperature, as anticipated in 1.1.4. We first measured electron density at different temperatures. This way the graph in figure 18, was obtained. It shows *n(T)* – the temperature dependency of electron density in 2DEG.

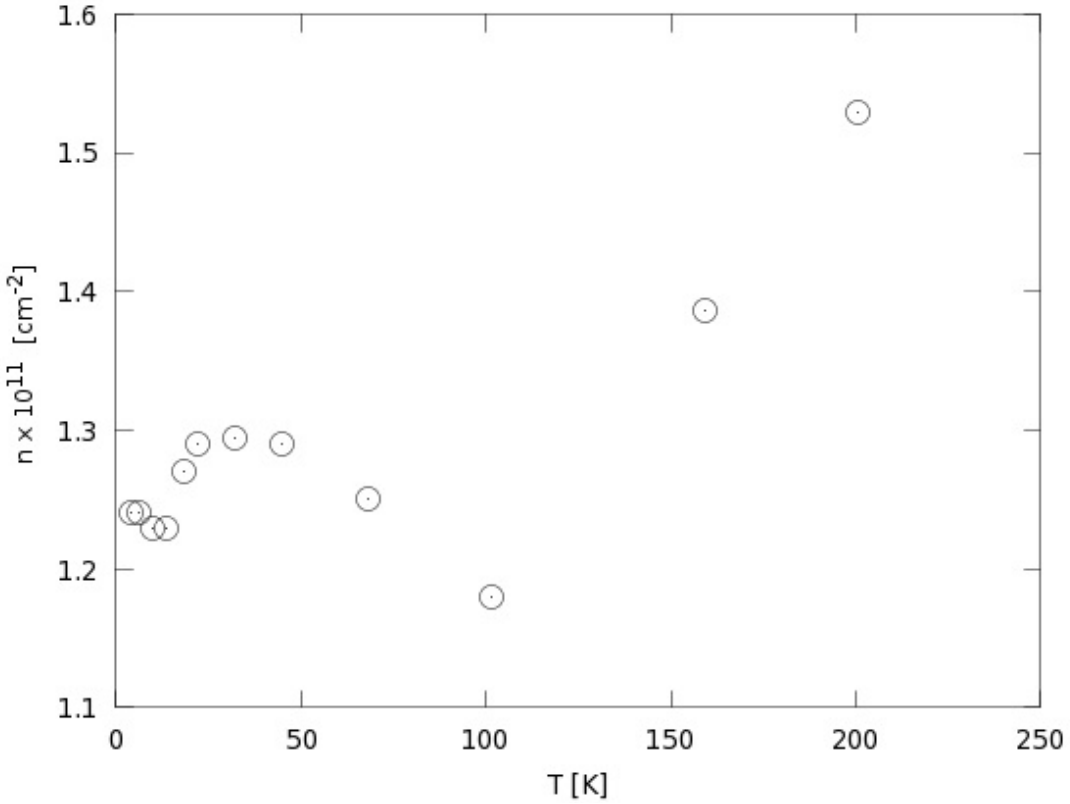

Figure 18: Graph depicting *n(T)* dependence showing that concentration is not constant and it indeed is temperature dependent.

Calculation of concentration n was based on equation 9, all what was needed was dependence of Hall voltage on magnetic field (which is linear) at a constant current flowing through the sample. Since we know that $n = \sigma_H B/e = IB/(eU_H)$ we fitted this linear curve with linear function. From this fit we obtained the constant of proportionality $const = B/U_H$. Therefore $n = const.(I/e)$. It is worth noting that we know both I – the current flowing though sample

(usually 1 to 10 μA) and *e* – elementary charge.

Second thing which was measured is the temperature dependance of longitudinal voltage *V(T)*. Character of such dependence measured on device is shown in figure 19.

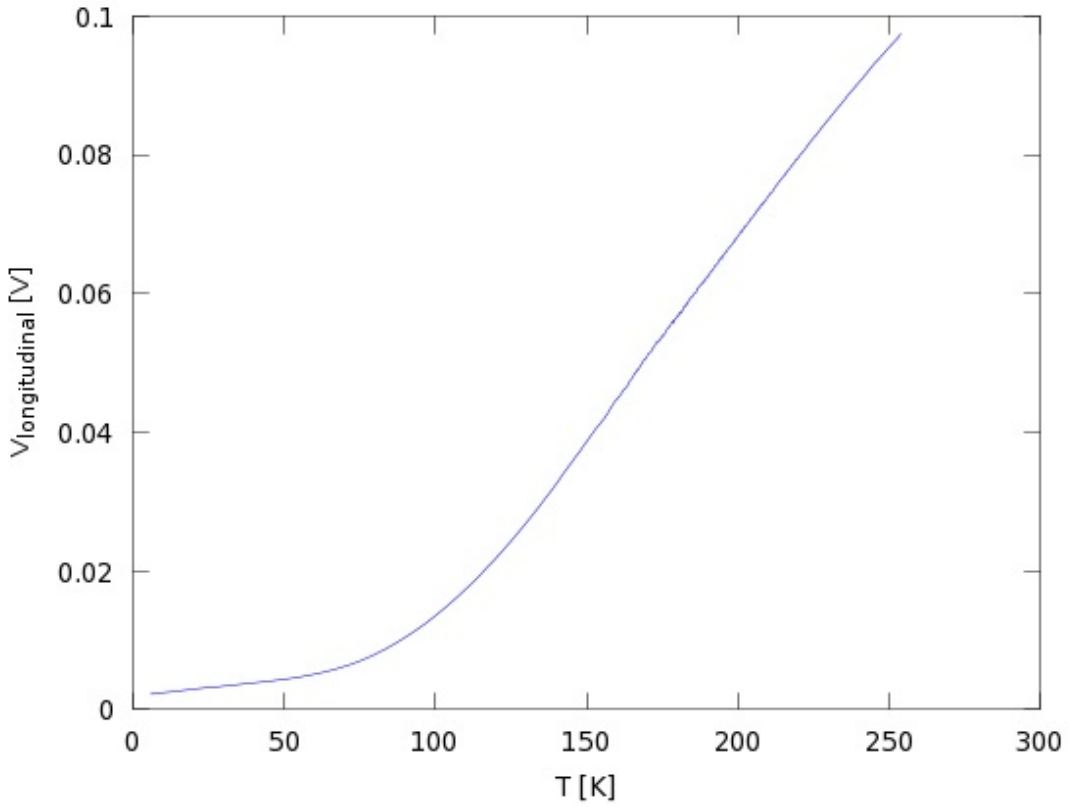

Figure 19: Character of measured *V(T)* dependence.

These two dependencies – *n(T)* and *V(T)*, are essentially all we need to have to determine the mobility of 2DEG. We know that the mobility is calculated via the equation - $\mu = \sigma/ne$ and this means that mobility is temperature dependent too. To obtain *μ(T)* dependence we had to divide *V(T)* dependence by *n(T)* dependence. Obviously there are not as many data points in *n(T)* dependence as there are in *V(T)* dependence. In order to compensate for that we used interpolation. One way to look at this fact is, that it complicates things, however the other way is to realize, that by

varying temperature, we can create 2DEG's with different mobilities, only by changing *T*, with no necessity to change the wafer.

The last remark of this part is that *n(T)* and *V(T)* dependencies were measured for all devices with different Hall-bar width. From this data $\mu(T)$ curves were created and thus we were able to obtain $\mu(w,T)$ dependence.

3.2.3 Methodology of checking the functionality of device

In part 3.1 there is description of experimental setup. *V(T)* was measured by method a). Each of eight devices was measured separately and each of these devices had three pairs of contacts that were used to measure the longitudinal voltage *V(T)*. Fourth pair was used as the current source. The scheme of the electrical circuit is shown in figure 20.

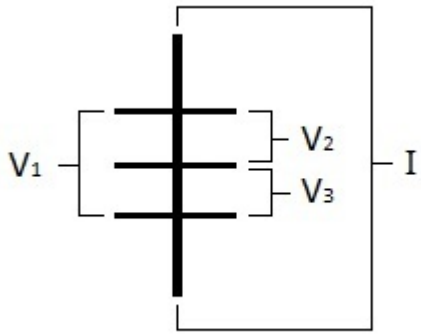

Figure 20: scheme of electrical circuit which was used to measure the V(T) dependence.

From this scheme it is obvious (because the distances between contacts are the same) that the following relation should hold:

$$V_1 = V_2 + V_3 \tag{36}$$

If this condition was met, the device was proclaimed to be functional, which especially means that the electric contacts are ohmic and there is no charge accumulation on them during cooling down. The maximum relative discrepancy from this condition was set to be 20%. Several other conditions, such as linearity of contacts of their low resistance can be sat as benchmark for functionality of device, however from experimental experience with this type of samples, condition 36 was chosen to be the most reliable as it combines both of mentioned conditions of the functionality of the device. Graph showing the character of condition 36 can be seen in figure 21.

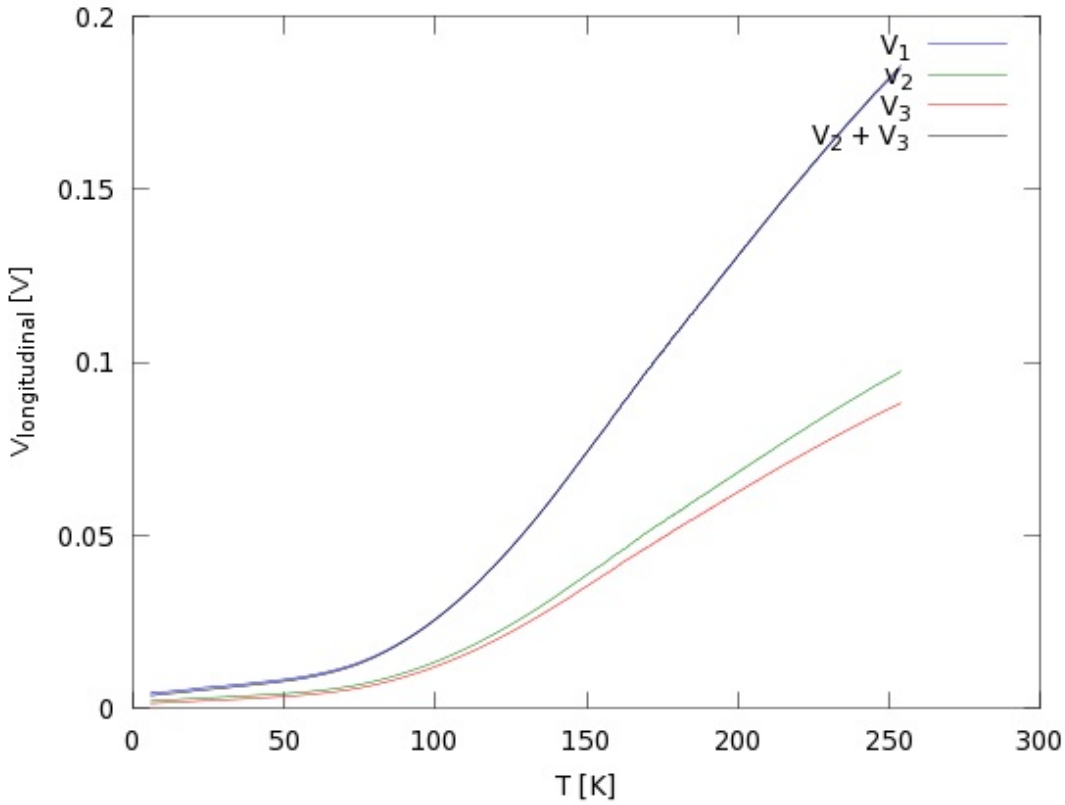

Figure 21: Graph showing the condition 36 - black line is sum of the bottom two lines (green V_2 and red V_3) and the blue one is actual measured voltage V_1.

The *n(T)* dependence was measured in the setup b). Since the assumption that 2DEG was homogeneously grown, all properties of the

2DEG, including the electron density should be the same for all devices. Therefore only one device was measured, to determine electron density n. Note that several approaches were used to determine the $n(T)$ dependence, all yielding basically the same results. First it was measure from 300 to 2K and then it was measure from 2 to 300K.

Last remark is, that only sample G096 was measured in this way, since it was more stable than sample E091.

3.2.4 Observations from temperature dependent results

In the graph in figure 22 one can see the overview 3D plot of $\mu(w,T)$ dependence, obtained as mentioned in section 3.2.1.

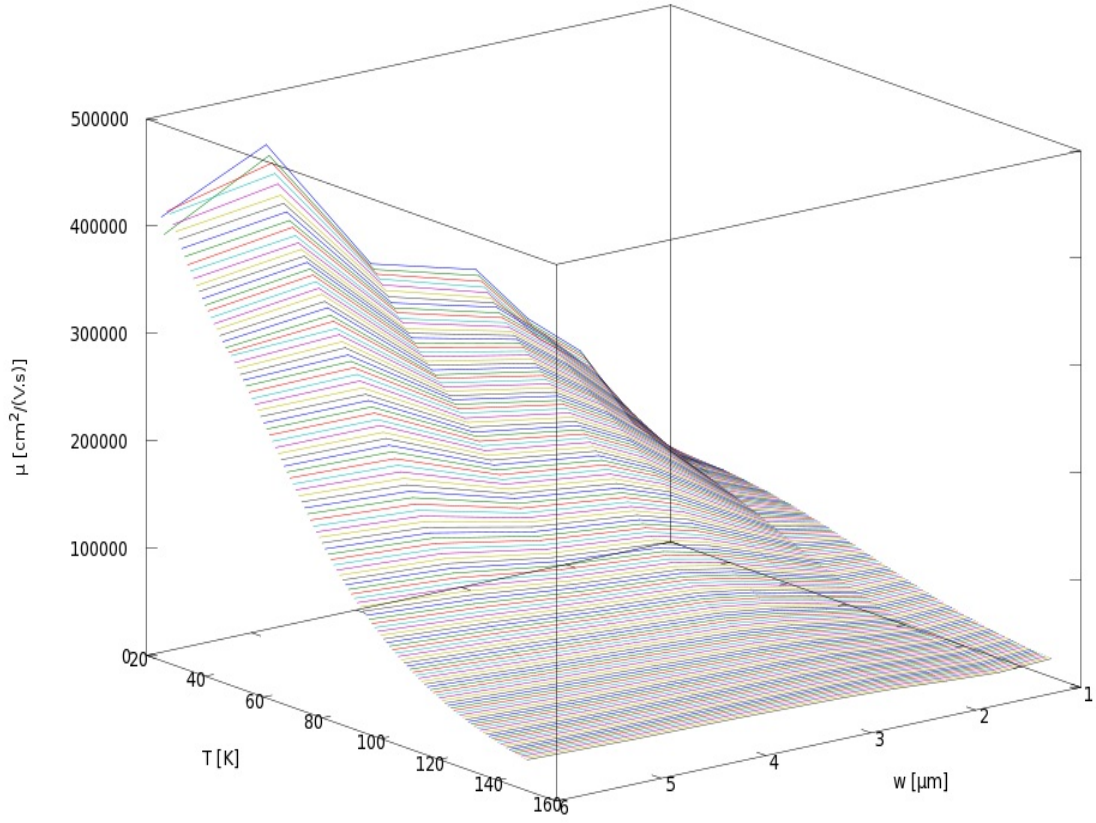

Figure 22: Graph showing $\mu(w)$ dependence for specified temperature region from 25 to 150K with step of 1K plotted in 3D as $\mu(w,T)$ dependence.

The immediate observation from this set of curves is that the default (meaning when 2DEG is unrestricted) mobility decreases with temperature since the scattering on phonons is enhanced (see 1.1.4). It is obvious that these dependencies are quite complex and in 3D graph they might not be very easy to comprehend. Therefore a new 3D graph was created where the mobilities are normalized. By normalizing, we mean that all curves are divided by the average mobility obtained from the last two (two with highest mobilities) data points of each curve. Normalized graph can be seen in the figure 23 below.

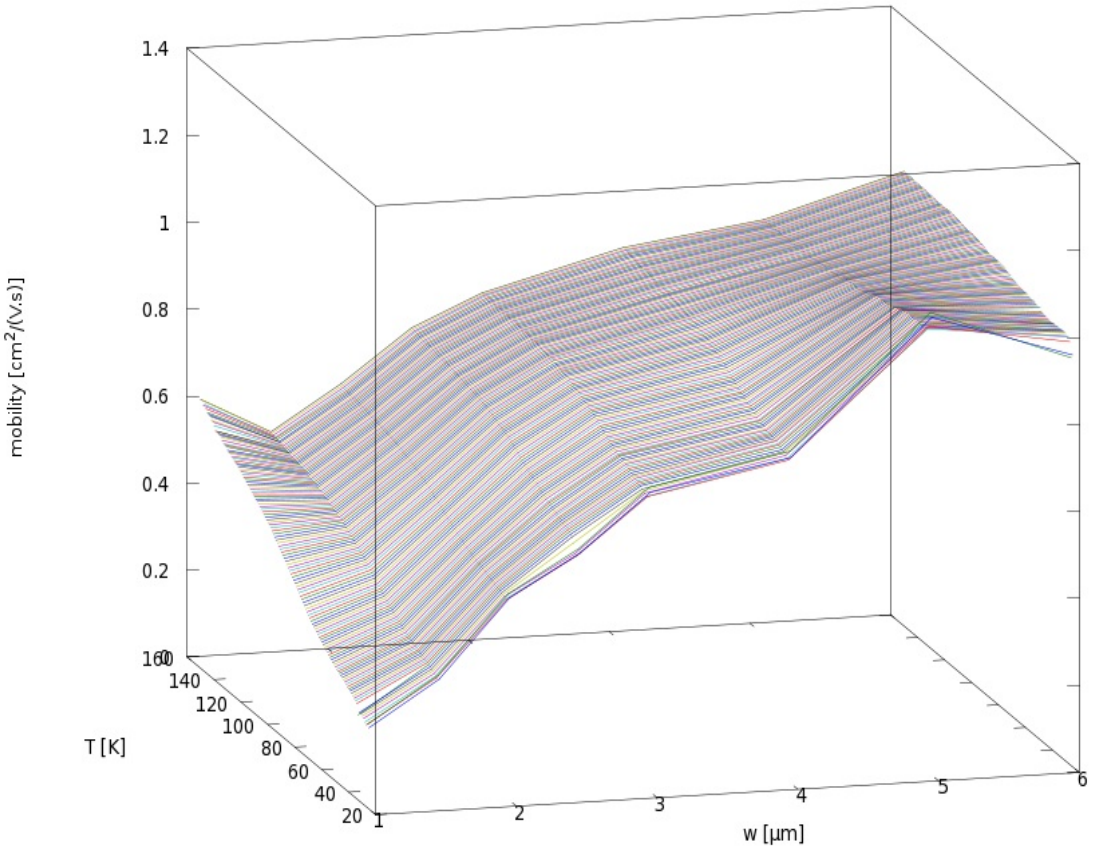

Figure 23: Normalized graph of $\mu(w,T)$ dependence emphasizing the regions where mobility drops for different curves.

Again several conclusions can be made. We expect the mobility to drop same as in figure 17 at 4K. This effect is present and strong for curves at

temperatures ranging from 25 to 60K. Significant drop in mobility can be observed even at 150K at Hall-bar width 2-3 μm, however at 25K it is at 4-5 μm. Other effect can be seen – the point where mobility starts to decrease significantly is less defined at higher temperatures. Theoretical explanation of these effects will be given in following section.

3.2.5 Discussion of temperature dependent results

The final data from figures 22 and 23 can be explained in two ways.

The first way is to use the Fermi-Dirac distribution. In this model the average velocity of particle is the Fermi velocity v_F but it is only true at 0K, despite of that, this model is widely used at low temperatures (below T_F). This model also predicts that high temperature curves from figure 23 should be constant since equation 35 states that at these temperatures the mean free path of electrons l_F is 0,3 μm which is narrower than the narrowest Hall-bar used. Moreover the Fermi velocity is temperature independent and therefore $l_F \approx \mu$. This however contradicts the obtained data. Because of that, at high temperatures, a second hypothesis should be used.

In Maxwell-Boltzmann distribution the average velocity $v_{TH} = \langle v \rangle$ is a function of temperature as can be seen from equation 23. If we now remember that mean free path of electrons can be written as $l_{MB} \approx \langle v \rangle \mu$ we immediately see, that while mobility drops with increasing temperature, the mean velocity raises. This means that the mean free path l_{MB} could be higher than l_F and in fact it is about 2-3 μm at 100K. This means that mobility should still drop at this Hall-bar width even at high temperatures as can be seen in figure 22.

Second effect present – worse defined point of significant decrease of mobility can be explained with Maxwell-Boltzmann velocity distribution too.

As before at low temperatures the system is described by Fermi-Dirac distribution. This means that only one velocity for particles is available – the Fermi velocity. This means the there is only one point at which the mean free path (since it's only one) of electrons is higher than Hall-bar width ergo the mobility drops.

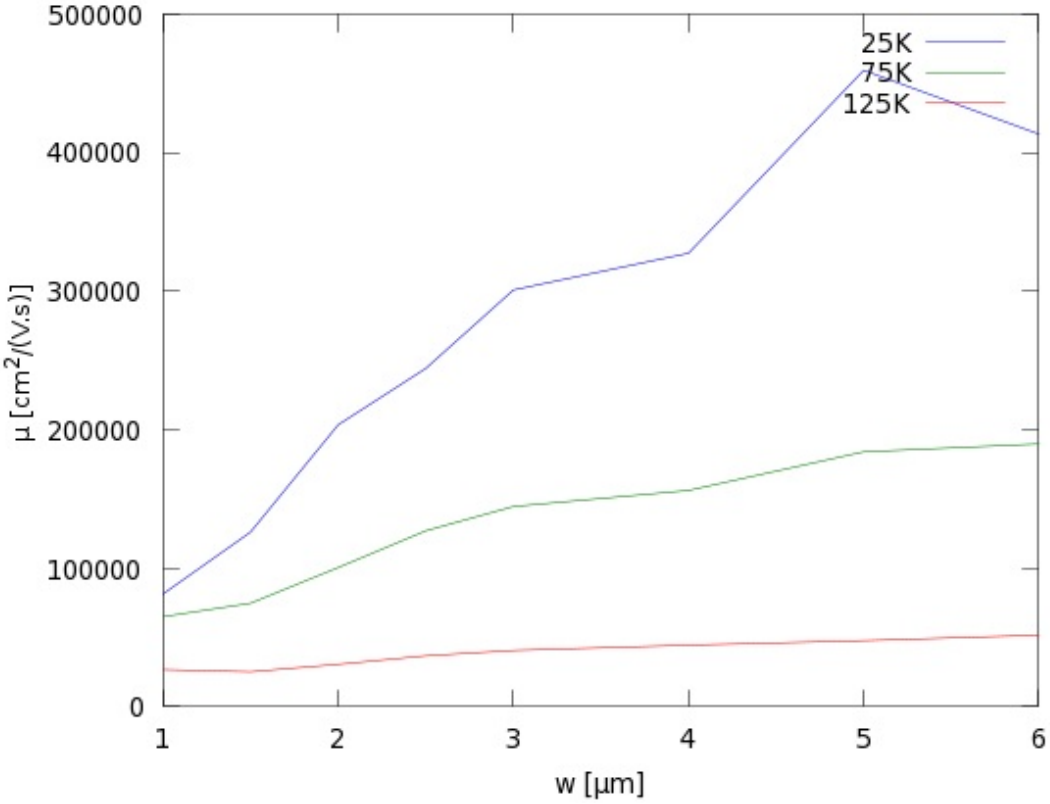

Figure 24: Graph comparing the μ(w) curves for three specified temperatures from the spectrum showing how the point where mobility drops significantly slightly moves to left whit respect to x axis.

However as it can be seen in figure 5, at high temperatures when system is described by Maxwell-Boltzmann distribution, more and more velocities are available to particles and there is a significant portion of particles flowing at velocities higher than average velocity. This means that there are many different mean free paths of electrons which in turn make the point where mobility drops significantly flatter as opposed to lower

temperatures where this point is sharp.

This effects of changing the mean free path of electrons and therefore of changing the point of mobility drop, and its worse definition can be comprehensively seen in figures 24 and 25.

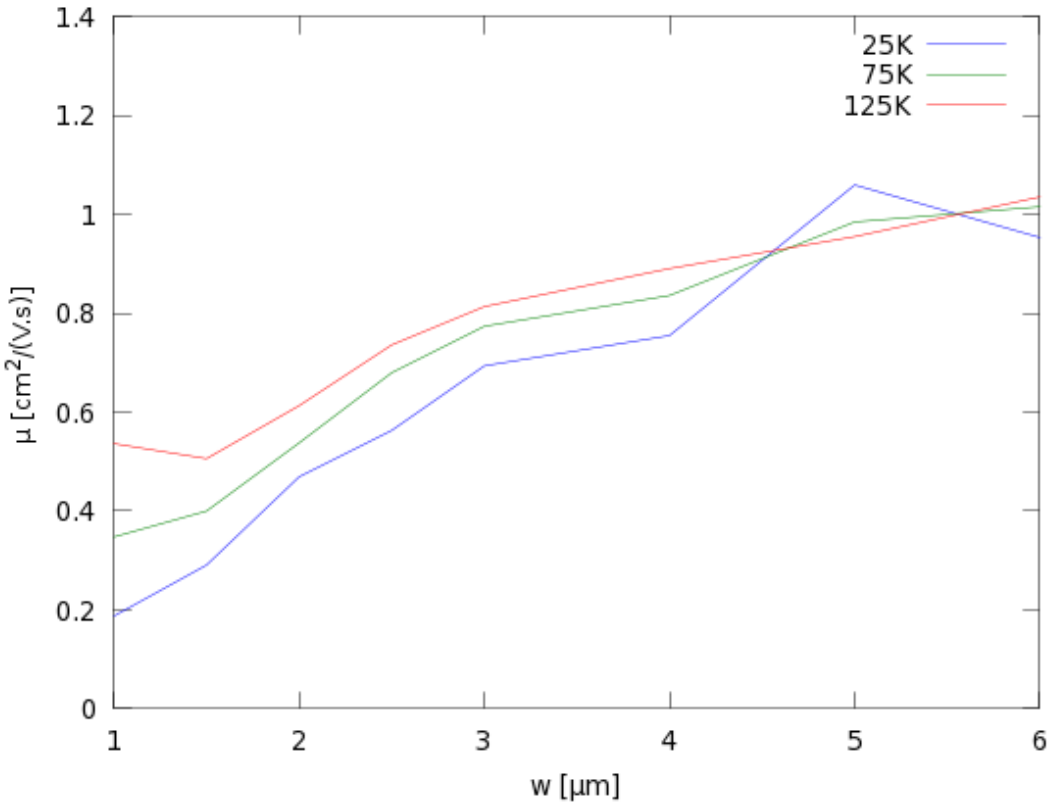

Figure 25: Graph comparing the normalized μ(w) curves for three specified temperatures from the spectrum showing how the point where mobility drops significantly is worse defined at high temperatures.

Final remark is that it was not specified how to point where mobility drops is defined. It is because it would be quite difficult to do so and it would be subjective. Moreover only qualitative explanations of new effects in experiment were given and therefore it is useless to explicitly define some way with which one can point to one specific point in graph. One way on how to look at this point is to look for a significant relative difference of mobilities between two neighboring data points.

3.3 Conclusion – Experimental part

It has been experimentally proven that mobility can indeed change because of spatial limitations – the idea that was first proposed by theoretical analysis of 2DEG. Figures that capture this result the most comprehensively are 17 and 22. It has also been shown, that mobility drops even at high temperatures. This fact has been explained thanks to the Maxwell-Boltzmann distribution which is valid at these temperatures contrary to the Fermi-Dirac distribution that is valid only at low temperatures.

4. Thesis conclusion

In chapter one of this thesis it was implied that the mobility of two dimensional electron gas can be influenced by the spatial dimensions to which such a system is placed. This idea was based on the Drude model. While old, it still has it's merit even today because it is possible to relatively easily and precisely to describe a quantum system for which proper description one would need much more complex theories. Based on the postulates given by P. Drude in 1900 we were able to derive key relation between the mobility and mean free electron path which is keystone to a proposed experiment. It's explanation would however proved to be difficult without the knowledge of Fermi-Dirac and Maxwell-Boltzmann distribution which take a key role in explanation of character of measured $\mu(w,T)$ dependence.

Both the experiment and the manufacture process took place at the Institute of Physics ASCR. As mentioned several times the experiment is very dependent on quality of devices which are even in spite of being manufactured by high end technologies like molecular beam epitaxy or electron lithography, often faulty. This led us to developing a new way with which to evaluate the data, during which new thermal effects, that influence the velocity and thus the mean free electron path, took place. This emphasized the fact, that the correct choice of statistical distribution used to describe the system and derive relations, is vital.

The experiment itself was made at extreme conditions that consist of high magnetic fields and low temperatures. These were achieved with standard experimental set-up where superconducting magnet is cooled by liquid helium. It has been qualitatively proven that mobility does indeed

depend on spatial dimensions and it has been found what the minimum width of a Hall channel is if one requires the mobility of such a system unchanged.. This result is important for spin Hall effect measurements [12, 13]. This transport phenomena was first observed in 1984 however it has only recently been studied in depth. It is believed that this effect could be exploited in a new type of electronics and it is therefore important to know the boundaries within which experiments can be made [14, 15, 16, 17, 18].

5. References

[1] Neil W. Ashcroft, N. David Mermin. Solid State Physics. United States of America: Thomson Learning, Inc. 1976. 826 s. ISBN 0-03-083993-9

[2] Peter Yu, Manuel Cardona. Fourth edition. Fundamentals of Semiconductors. Springer, 2010. 795s. ISBN 3642007104

[3] G. E. Stillman, C. M. Wolfe. Electrical characterization of epitaxial layers. Lincoln Laboratory, Massachusetts Institute of Technology, Lexington, Mass. 02173 (U.S.A.), 1975.

[4] W. Walukiewicz. Electron mobility in modulation-doped heterostructures. H. E. Ruda, J. Jagowski, H.C. Gatos. Massachusetts Institute of Technology, Cambridge, Massachusetts 02139, 1984

[5] Herbert B. Callen. Thermodynamics and introduction to thermostatics. Wiley India Pvt. Limited, 2006. 512a. ISBN 8126508124

[6] Charles Kittel. Introduction to Solid State Physics. Eight edition. University of California, Berkeley. 2005. 703s. ISBN 0-471-41526-X

[7] J. Pavel Středa, Elektronový transport v kvantových systémech, skriptum, Fyzikální ústav AVČR.

[8] Wikipedia. Molecular beam epitaxy. Poslední změna 11.2.2014 17:50 [cit. 3.5.2014]. Dostupné z: http://en.wikipedia.org/wiki/Molecular-beam_epitaxy

[9] Wikipedia. Photolithography. Poslední změna 12.1.2014 19:33 [cit. 18.5.2014]. Dostupné z: http://en.wikipedia.org/wiki/Photolithography

[10] František Matějka. Praktická elektronová litografie. UTP AV ČR v.v.i: Brno, 2013. ISBN 978-80-87441-04-6

[11] R.S. Šafrata a kol., Fyzika nízkých teplot, MatfyzPress, Praha 1998, ISBN 80-85863-19-7

[12] J. Wunderlich. Spin-injection Hall effect in a planar photovoltaic cell. A.C. Irvine, Jairo Sinova, B. G. Park, L.P. Zârbo, X. L. Xu, B. Kaestner, V. Novák and T. Jungwirth. Nature Physics, Macmillan Publishers Limited, 2009.

[13] J. Wunderlich. Experimental Observation of the Spin-Hall Effect in a Two-Dimensional Spin-Orbit Coupled Semiconductor System. B. Kaestner, J. Sinova, T. Jungwirth. PHYSICAL REVIEW LETTERS, The American Physical Society, 2005.

[14] Petr Němec. Cesta ke spinovému tranzistoru. Matematicko-fyzikální fakulta, Univerzita Karlova v Praze, 2012

[15] Claude Chappert, Albert Fert, Frédéric Nguyen van Dau. The emergence of spin electronics in data storage. Review articles, Insight, Nature Publishing Group, 2007

[16] Dirk Grundler. Spintronics. Physics World, April 2002

[17] Sankar Das Sarma. Spintronics. American Scientist, Volume 89, 2001

[18] David D. Awschalom. Spintronika. Michael E. Flatté a Nitin Samarth. Scientific American české vydání, 2002